Received: 10 June 2017 | Revised and accepted: 26 January 2018 | Uncorrected manuscript published: 13 February 2018

DOI: 10.1111/tra.12552

WILEY Traffic

ORIGINAL ARTICLE

Phagocytosis of antibody-opsonized tumor cells leads to the formation of a discrete vacuolar compartment in macrophages

Ramraj Velmurugan[1,2,3] | Sreevidhya Ramakrishnan[1,4] | Mingin Kim[5] | Raimund J. Ober[1,4] | E. Sally Ward[1,2]

[1]Department of Molecular and Cellular Medicine, Texas A&M University Health Science Center, College Station, Texas

[2]Department of Microbial Pathogenesis and Immunology, Texas A&M University Health Science Center, Bryan, Texas

[3]Biomedical Engineering Graduate Program, University of Texas Southwestern Medical Center, Dallas, Texas

[4]Department of Biomedical Engineering, Texas A&M University, College Station, Texas

[5]Medical Science Graduate Program, Texas A&M University Health Science Center, College Station, Texas

Correspondence
Raimund J. Ober, Department of Biomedical Engineering, Texas A&M University, College Station, TX 77843.
Email: raimund.ober@tamu.edu
E. Sally Ward, Department of Molecular and Cellular Medicine, Texas A&M University Health Science Center, College Station, TX 77843.
Email: sally.ward@tamu.edu

Funding information
National Institutes of Health, Grant/Award number: R01GM085575; Cancer Prevention and Research Institute of Texas, Grant/Award numbers: RP110441, RP140141

Despite the rapidly expanding use of antibody-based therapeutics to treat cancer, knowledge of the cellular processes following phagocytosis of antibody-opsonized tumor cells is limited. Here we report the formation of a phagosome-associated vacuole that is observed in macrophages as these degradative compartments mature following phagocytosis of HER2-positive cancer cells in the presence of the HER2-specific antibody, trastuzumab. We demonstrate that this vacuole is a distinct organelle that is closely apposed to the phagosome. Furthermore, the size of the phagosome-associated vacuole is increased by inhibition of the mTOR pathway. Collectively, the identification of this vacuolar compartment has implications for understanding the subcellular trafficking processes leading to the destruction of phagocytosed, antibody-opsonized cancer cells by macrophages.

KEYWORDS

antibodies, lysosome, macrophages, phagosome, vacuole

1 | INTRODUCTION

The process by which eukaryotic cells engulf and degrade particulate matter is known as phagocytosis.[1] Specialized phagocytes such as macrophages are particularly active in this process. Fusion of endolysosomal compartments with the maturing phagosome as it acidifies results in the delivery of degradative enzymes followed by the destruction of phagosomal contents.[2] Phagocytosed targets, such as mammalian cells, that approach the size of the phagocyte comprise a large proportion of the cellular content of a phagocyte, and as such, present unique challenges for degradation due to their relatively large size. By contrast with beads, which are typically used as models for the study of phagocytic processes, phagocytosed cells contain degradable content. Consequently, the release of metabolites such as amino acids during the degradation process could induce osmotic

Ramraj Velmurugan and Sreevidhya Ramakrishnan contributed equally to this study.

stress within the phagosome, causing it to increase in volume.[3] Hence, effector cells may employ specific mechanisms during the degradative processing of cells within phagosomes in order to limit cellular stress.

The mechanistic target of rapamycin (mTOR) is a component of the mTOR complex 1 that localizes to lysosomes and acts as a sensor of nutrient availability and growth factor signaling.[4,5] Specifically, this pathway is responsive to the accumulation of amino acids in the lysosomal lumen.[6] This suggests that the degradation of cells within phagosomes, or in entotic vacuoles that arise from live cell engulfment by neighboring cells ("entosis"),[7] may be coordinated by the mTOR pathway, particularly in cases where the degradation process leads to amino acid release.[8] Nevertheless, recent studies have revealed the complexity of the pathways, including mTOR-independent processes, that play a role in entotic vacuole or phagosome maturation and fission to generate lysosomes.[9–12]

The study of cellular phagosomes is directly relevant to antibody-dependent cellular phagocytosis (ADCP) of targets such as tumor cells. Antibodies represent a rapidly expanding class of therapeutics for the treatment of cancer.[13] The recognition of tumor-specific antigens by therapeutic antibodies results in coating, or opsonization, of the cancer cells which can lead to ADCP.[14,15] The presence of macrophages as the most abundant immune cell type in the majority of tumors[16] suggests that macrophage-mediated ADCP may contribute to the anti-tumor effects of antibodies. Although macrophages can lead to pro-tumorigenic consequences, results from multiple studies are consistent with a contribution of macrophage-mediated effector activity to tumor cell death.[17–23] Furthermore, antigen can be processed from these phagosomes and presented in the context of major histocompatibility complex class I or II molecules to cognate T cells.[24,25] Hence, studying the maturation pathway of cellular phagosomes is expected to be of direct relevance to the successful use of therapeutic antibodies and induction of anti-tumor immunity.

In the current study, we have analyzed the fate of phagosomes containing antibody-opsonized cancer cells within macrophages. Interestingly, we observe the formation of a distinct phagosome-associated vacuole during phagosome maturation. This phagosome-associated vacuole is separated from the phagosome by a barrier that selectively restricts diffusion of solutes between the 2 compartments based on their size. Furthermore, vacuoles are not detected following the phagocytosis of antibody-opsonized beads, indicating that cellular components within the phagosome may regulate vacuole formation. In addition, vacuole enlargement was observed in the presence of the mTOR inhibitor, torin 1. Collectively, our results suggest that this vacuole is a common feature associated with the degradation of cellular targets by phagocytes.

2 | RESULTS

2.1 | Identification of a phagosome-associated vacuole

Initially, we used live cell microscopy to analyze the phagocytic process involving J774A.1 macrophages as effectors and MDA-MB-453 breast cancer cells as targets. MDA-MB-453 cells were opsonized with Alexa 555-labeled HER2-specific antibody (trastuzumab) and co-incubated with macrophages that had been preloaded with Alexa 647-labeled dextran to identify lysosomes. At approximately 3 hours following phagocytosis, we observed the formation of a vacuole-like structure with a clear phase-contrast profile adjacent to the phagosome (Figure 1A, Movie S1, Supporting information). Time-lapse images showed a gradual increase in the size of this vacuole over 2 to 6 hours (Figure 1A). We observed that the vacuole and phagosome were positive for both Alexa 647 and Alexa 555 fluorophores (Figure 1B, Movie S1), indicating that the vacuole contains both lysosomal components and opsonizing antibody (fragments) derived from the macrophages and cancer cells, respectively. In addition, the proportion of labeled dextran derived from macrophage lysosomes that is associated with phagosome/vacuole compartments relative to that in "free" lysosomes in macrophages was quantitated and ranged from 20% to 60% (n = 9), suggesting a high frequency of lysosomal fusion with the phagosome and/or vacuole (Figure 1C).

We next investigated the time-course of the formation of the vacuole. Antibody-opsonized target cells were mixed with macrophages, and intravenous immunoglobulin (IVIG) was added to the conjugates following 1 hour to prevent further phagocytosis (by competitive inhibition of Fcγ receptor binding[17]). The number of phagosomes containing an associated vacuole following a 2-, 4-, 6- or 8-hour incubation period after the addition of IVIG were quantitated by microscopy analyses. This quantitation showed that the percentage of phagocytosed cells with associated vacuoles is maximal at ~75% (n = 150) at 6 hours following the addition of IVIG to block further phagocytosis, and this percentage decreases to ~50% (n = 148) at 8 hours (Figure 1D).

We also analyzed whether vacuoles form following the engulfment of apoptotic bodies by macrophages. Target cells were exposed to ultraviolet (UV) irradiation to induce apoptosis, and the resulting apoptotic bodies were incubated with macrophages for 7 hours followed by microscopy analyses (n = 68 apoptotic vacuoles; Figure 1E). Flow cytometric analyses using fluorescently labeled annexin V confirmed the induction of apoptosis (Figure S1). These studies revealed that vacuoles form adjacent to phagosomes containing apoptotic bodies. Interestingly, by contrast with phagocytosed cancer cells or apoptotic bodies, vacuoles were not detected in macrophages that had phagocytosed streptavidin coated, 10-μm diameter latex beads coupled to biotinylated trastuzumab (n = 128 phagocytosed beads; Figure 1F).

2.2 | The phagosome and vacuole are LAMP-1+ and their contents are redistributed into lysosomes

Consistent with the fusion of lysosomes with maturing phagosomes and associated vacuoles, staining of macrophages following phagocytosis of cancer cells with a LAMP-1-specific antibody demonstrated that the limiting membranes of both phagosomes and vacuoles have associated LAMP-1 (Figure 2A). By contrast with the analyses of lysosomal markers, pulsing of J774A.1 macrophage: MDA-MB-453 co-cultures with Alexa 555-labeled transferrin indicated that phagosomes and associated vacuoles do not have detectable levels of this early/recycling endosomal marker (Figure 2B).

To further characterize the fate of the vacuole, co-cultures of macrophages and opsonized cancer cells were incubated for 6 hours and phagosome-associated vacuoles in these samples were analyzed by

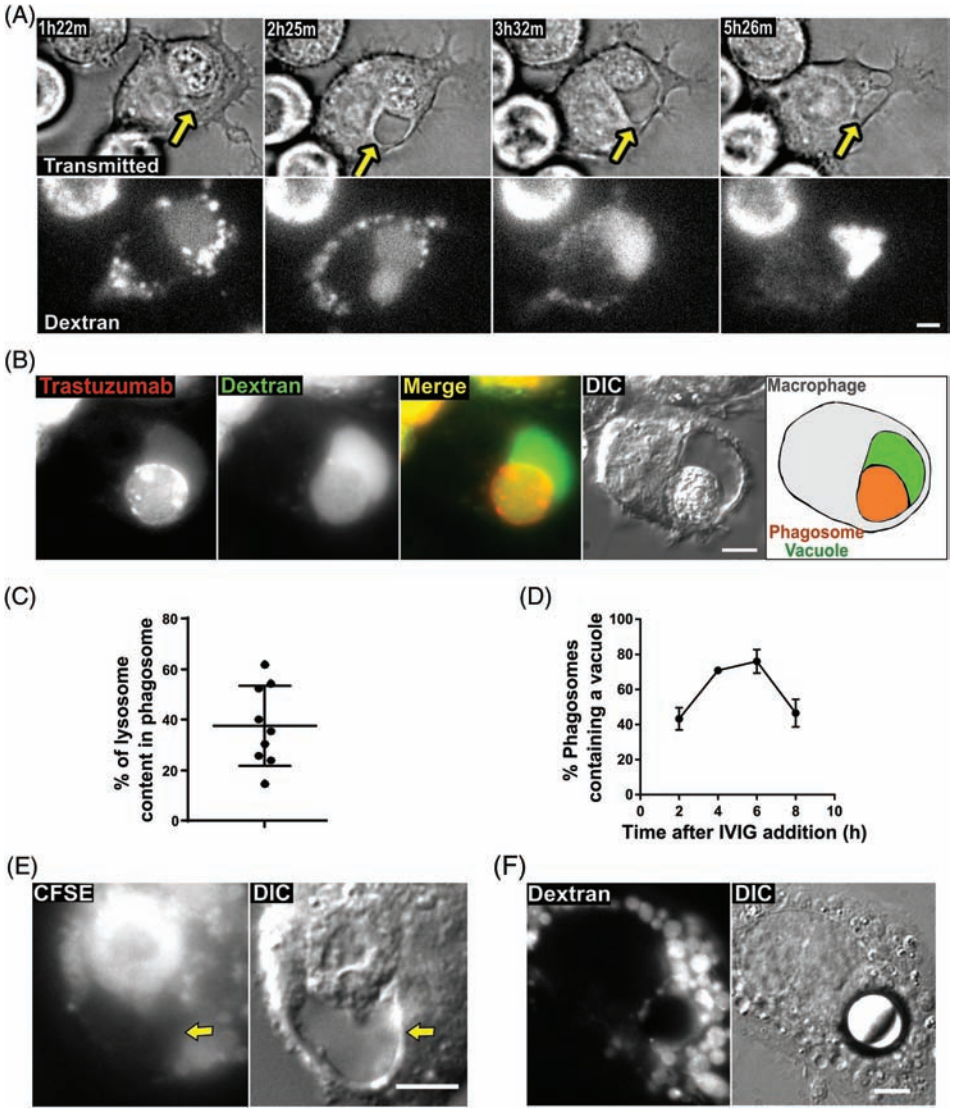

FIGURE 1 Phagosomes containing cancer cells have associated vacuoles. A, MDA-MB-453 cancer cells were opsonized with Alexa 555-labeled trastuzumab and co-incubated with J774A.1 macrophages for 1 hour. The macrophages were preloaded with Alexa 647-labeled 10 kDa dextran. A macrophage containing a phagocytosed target cell was identified and imaged live for 12 hours. The images show transmitted light and dextran fluorescence for this macrophage at the indicated time points following the start of imaging. B, Fluorescent and DIC images of a phagosome from a sample prepared as in A following a 4.5-hour incubation. Alexa 555 (trastuzumab) is pseudocolored red, and Alexa 647 (dextran) is pseudocolored green. The right-hand panel shows a schematic diagram of the approximate location of the phagosome-associated vacuole (green), the phagosome containing the corpse of the target cell (orange) and the boundary of the macrophage (gray). C, J774A.1 macrophages were preloaded with Alexa 488-labeled 10 kDa dextran and co-incubated with MDA-MB-453 cancer cells opsonized with trastuzumab for 6 hours. z-stack images of cells (n = 9 phagosomes) were taken and the proportion of labeled dextran associated with the phagosome/vacuole compartments relative to that in "free" lysosomes in macrophages was quantitated. Error bars represent SEs. D, MDA-MB-453 cells were opsonized with Alexa 488-labeled trastuzumab and co-incubated with J774A.1 macrophages preloaded with Alexa 647-labeled 10 kDa dextran. After co-incubation for 1 hour, 10 mg/mL IVIG was added to prevent further phagocytic activity. Fluorescent and DIC images of the phagosomes were then taken at the indicated time points following IVIG addition, and the phagosomes with an associated vacuole were counted. Error bars represent SEs. E, MDA-MB-453 cancer cells were preloaded with FITC-labeled carboxyfluorescein succinimidyl ester (CFSE), UV-irradiated for 3 hours to induce apoptosis and subsequently co-incubated with J774A.1 macrophages for 1 hour followed by the addition of 10 mg/mL IVIG and incubation for a further 6 hours followed by imaging. Fluorescent and Differential Interference Contrast (DIC) images are shown. F, Streptavidin-coated beads (10 μm diameter) were opsonized with biotinylated trastuzumab, washed and added to J774A.1 macrophages. The macrophages were preloaded with Alexa 647-labeled 10 kDa dextran. The cells were subsequently incubated for 1 hour followed by the addition of 10 mg/mL IVIG and incubation for a further 6 hours followed by imaging. Fluorescent and DIC images are shown. Yellow arrows in A and E indicate the position of the vacuole. For panels A, B, E and F, images of representative cells from at least 12 cells are shown. Data for all panels are representative of at least 2 independent experiments. Scale bars = 5 μm

long-term live cell imaging. In this experiment, the lysosomes of the target cells were labeled instead of trastuzumab, to distinguish phagocytosis from trogocytosis ("nibbling," in which membrane fragments, but not lysosomes of the target cell accumulate in macrophages).[17,26,27] Time-lapse images from long-term imaging reveal that as the phagosome-associated vacuoles begin to decrease in size around 8 hours, the

dextran originating from the target cell, which was initially present in both the phagosome and the vacuole, redistributes throughout the lysosomal network of the macrophage during the following 14 hours (Figure 2C, Movie S2). Similar results were obtained when the lysosomes in cancer cells, but not in macrophages, were labeled with Alexa 488-labeled dextran (Figure S2). These analyses indicate that the phagosome-associated vacuole is a temporary structure formed during the maturation of phagosomes and that the contents of the vacuole are subsequently redistributed into the lysosomal network.

2.3 | The phagosome and vacuole are discrete compartments

To investigate whether the vacuole is lysosomal in nature, we treated samples containing phagosome-associated vacuoles with the dye LysoTracker Red, which is membrane permeant and accumulates through trapping by protonation in acidic compartments, including lysosomes.[28] Interestingly, although the phagosome was, as expected from earlier studies,[8] positive for LysoTracker, the dye was undetectable in the phagosome-associated vacuole (Figure 3A). To further explore the properties of the vacuole, we treated the samples with LysoSensor Blue DND-192, that is also membrane permeant and protonated in acidic compartments.[29] As expected, the phagosome was positive for LysoSensor Blue fluorescence. Although the intensity of the LysoSensor staining in the vacuole was lower relative to that in the phagosome, LysoSensor signal could be detected in the vacuolar region, by contrast with very low to undetectable levels of LysoTracker signal (Figure 3B).

Although the vacuole had very low to undetectable levels of fluorescent signal from LysoTracker, we detected higher levels of fluorescence around the limiting membrane of the vacuole, suggesting that this membrane might be multilamellar (Figure 3A, inset). Hence, to further understand the ultrastructural properties of the vacuole, we prepared specimens of phagocytosed target cells for analysis using transmitted electron microscopy (EM). EM images showed that the vacuoles had very low density compared with the surrounding cytoplasm, while the target cell corpse had a morphology analogous to that observed by others for cellular phagosomes (Figure 3C).[30] The EM images of the vacuole also displayed membrane-limited subcompartments within this structure. To determine whether these membrane subdivisions are also found inside phagosome-associated vacuoles in live specimens, the target cells were labeled with the membrane dye FM 4-64FX before co-incubation with the macrophages. Analyses of phagosome-associated vacuoles with these FM dye-labeled targets revealed that this dye labeled the limiting membranes of subcompartments within the vacuolar region (Figure 3D).

To further investigate whether the phagosome and vacuole have distinct properties, we preloaded macrophages with an equimolar mixture of Alexa 488- and pHrodo Red-labeled 10 kDa dextran prior to co-incubation with antibody-opsonized tumor cells. The fluorescent signal of pHrodo Red increases as the pH becomes more acidic, whereas that of Alexa 488 is constant across a broad pH range of 4 to 10.[31] The ratios of fluorescent intensities of pHrodo Red:Alexa 488 in the phagosomes and vacuoles were determined, and for 60% (n = 110) of vacuoles the ratio was found to be lower than those of adjacent phagosomes, whereas for the remaining 40% the ratio was similar in both compartments (Figures 3E and S3). Collectively, these data suggest that the pH of the vacuole can be higher than that of the phagosome.

2.4 | The vacuole and phagosome are separated by a semi-permeable membrane

In combination with the EM data, the differential accumulation of LysoTracker and LysoSensor in the vacuole suggested that the phagosome and vacuole are discrete compartments. However, the accumulation of Alexa Fluor dye following phagocytosis of cancer cells opsonized with Alexa 555-labeled trastuzumab indicated that some macromolecules could transfer between the compartments. To investigate whether the barrier between these 2 compartments limits movement of solutes above a particular size threshold, we labeled the surface of target cells with QDot 655-labeled trastuzumab. These quantum dot nanoparticles have an approximate diameter of 20 nm.[32] Vacuoles associated with phagosomes containing target cells did not contain any quantum dots, indicating that the barrier is impermeant to these nanoparticles (Figure 4A).

Previous studies have used fluorescently labeled dextrans of different molecular weights to investigate the effect of size on subcellular transport processes (e.g., phagosomal-lysosomal and lysosomal fusion).[33,34] We therefore labeled the lysosomes of the macrophage with fluorescent dextrans of different molecular weights (65-85 kDa, referred to as 75 kDa, and 155 kDa) and subsequently co-incubated these cells with trastuzumab-opsonized cancer cells. As a control, lysosomes of the macrophage were also labeled with 10 kDa dextran. When 75 and 10 kDa dextrans were preloaded together in macrophage lysosomes, both dextrans accumulated in the vacuoles (n = 40) to similar levels (Figure 4B). However, when 155 and 10 kDa dextrans were preloaded together in macrophage lysosomes, the accumulation of 155 kDa dextran was substantially lower compared with 10 kDa dextran in the majority (81%, n = 71 phagosomes) of the vacuole compartments. The differential vacuolar localization of these dextrans and quantum dot nanoparticles indicates that the barrier between the phagosome and the vacuole can exclude the transfer of molecules/particles above a particular size threshold.

2.5 | Formation of the phagosome-associated vacuole is independent of the effector or target cell type

Using LysoTracker to differentiate the phagosome-associated vacuole from the phagosome, we investigated whether the phagosome-associated vacuole is observed for other macrophage:cancer cell couples. Target cells were co-incubated with bone marrow-derived macrophages and human monocyte-derived macrophages. Similar vacuole structures were associated with phagosomes for all macrophage types (Figure S4A,B). The vacuole was also observed when trastuzumab-opsonized SK-BR-3 breast cancer cells or anti-CD20 (rituximab)-opsonized Raji B cells were used as targets, indicating that the formation of this structure is not dependent on the target cell type or the specificity of the opsonizing antibody (Figure S4C).

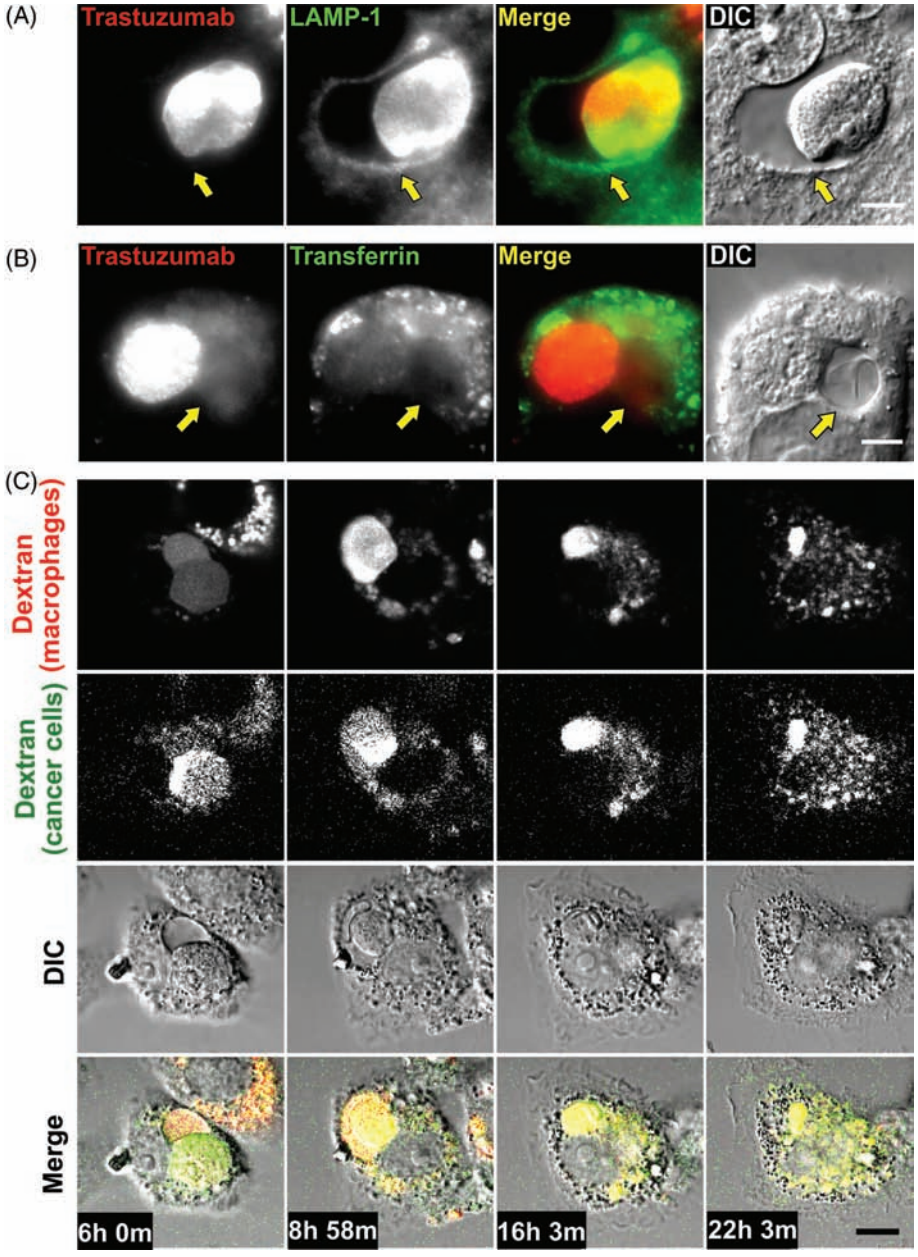

FIGURE 2 The phagosome and vacuole are LAMP-1+ and their contents are redistributed throughout the lysosomal network of the macrophage. A, MDA-MB-453 cancer cells were opsonized with Alexa 488-labeled trastuzumab and co-incubated with J774A.1 macrophages for 1 hour followed by addition of 10 mg/mL IVIG and incubation for a further 6 hours. Cells were fixed, permeabilized, and LAMP-1 was detected using a LAMP-1-specific antibody followed by an Alexa 647-labeled secondary antibody. Fluorescent and DIC images are shown, with Alexa 488 (trastuzumab) pseudocolored red, and Alexa 647 (LAMP-1) pseudocolored green. B, MDA-MB-453 cancer cells were opsonized with Alexa 488-labeled trastuzumab and co-incubated with J774A.1 macrophages for 1 hour followed by addition of 10 mg/mL IVIG and incubation for a further 6 hours. Cells were pulsed with 10 μg/mL Alexa 555-labeled human transferrin at 37°C for the last 10 minutes of the incubation and then cells were washed and imaged as live cells. Fluorescent and DIC images are shown, with Alexa 488 (trastuzumab) pseudocolored red and Alexa 555 (transferrin) pseudocolored green. C, MDA-MB-453 cancer cells opsonized with trastuzumab were co-incubated with J774A.1 macrophages. The cancer cells were preloaded with Alexa 555-labeled 10 kDa dextran (pseudocolored green), and the macrophages were preloaded with Alexa 488-labeled 10 kDa dextran (pseudocolored red). Imaging (fluorescence and DIC) was initiated 6 hours following the start of the co-incubation. The panels show 4 frames from the time series, with times corresponding to each frame indicated. Yellow arrows in A and B indicate the position of the vacuole. Images of representative cells from at least 14 cells and 2 independent experiments are shown. Scale bar = 5 μm

2.6 | The mTOR pathway regulates the size of phagosome-associated vacuoles

The mTOR pathway affects lysosomal biogenesis, with high levels of amino acids leading to the inhibition of transcription of genes associated with lysosome formation.[5,35,36] In addition, mTOR inhibition has been shown to reduce fission of the entotic vacuole, a structure that is observed following engulfment of live (non-opsonized) cells by adjacent cells during carcinogenesis or development.[8] We therefore investigated whether treatment with the mTOR inhibitor, torin 1, affected the size of the vacuoles. Phagosome-associated vacuoles were observed in the presence of torin 1 (Figure 5A), and their size

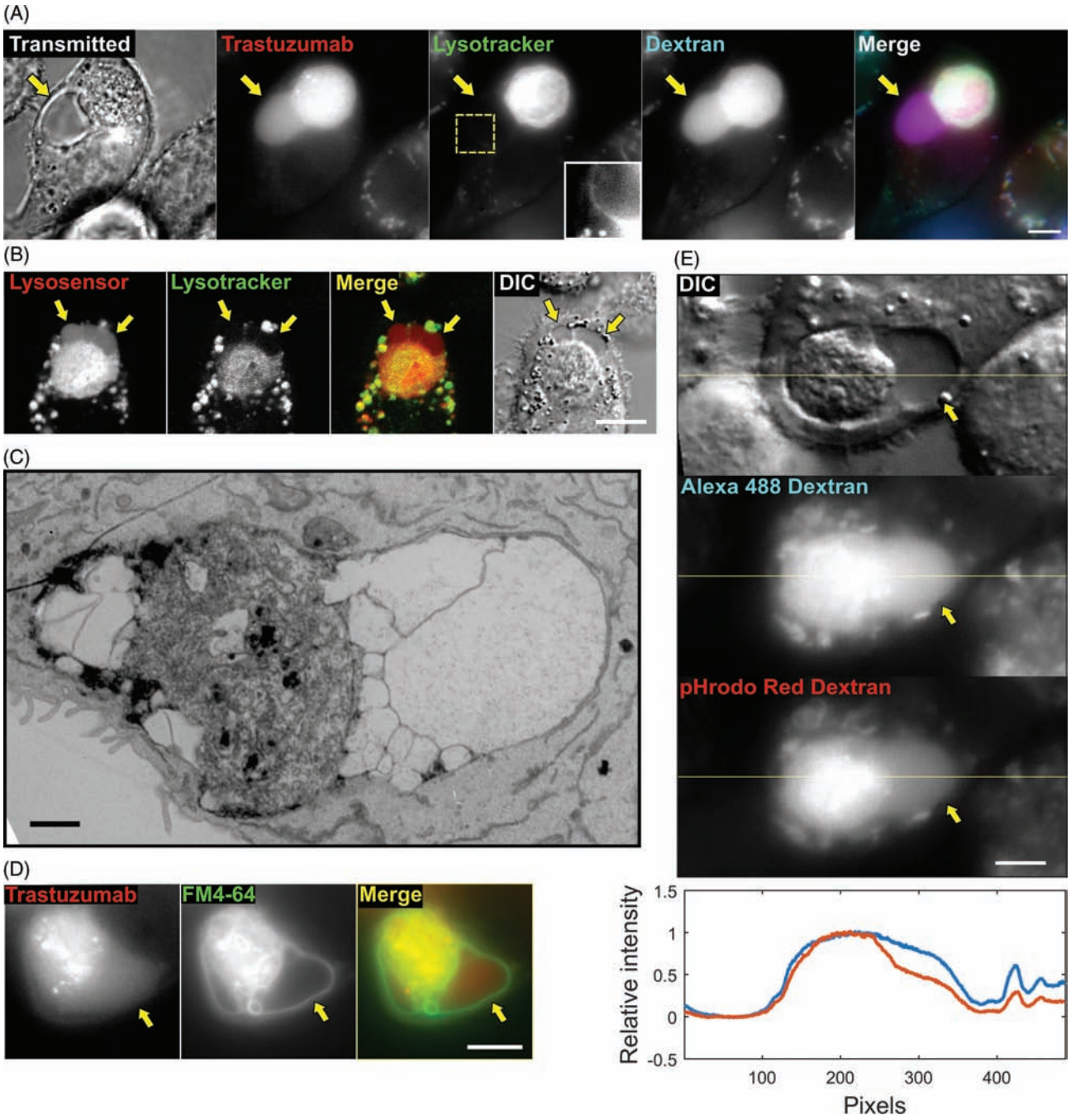

FIGURE 3 The vacuole contains membranous subcompartments. A, MDA-MB-453 cells were opsonized with Alexa 488-labeled trastuzumab (pseudocolored red), added to J774A.1 macrophages preloaded with Alexa 647-labeled 10 kDa dextran (pseudocolored blue), and incubated for 13 hours. LysoTracker Red (pseudocolored green) was then added to the medium, and the cells were imaged (transmitted light and fluorescence). The inset in the center panel corresponds to an enlargement of the cropped area (dotted lines) to show the region of interest with enhanced contrast. B, MDA-MB-453 cells were opsonized with trastuzumab and co-incubated with J774A.1 macrophages, and incubated for 6 hours. LysoSensor Blue (pseudocolored red) and LysoTracker Red (pseudocolored green) were then added to the medium, and the cells were imaged (fluorescence and DIC). C, MDA-MB-453 cells opsonized with trastuzumab were added to J774A.1 macrophages, incubated for 6 hours, fixed and processed for EM. An EM image of a phagosome with associated vacuoles is shown (representative of 9 phagosomes). D, MDA-MB-453 cells were harvested, labeled with the FM 4-64FX dye (pseudocolored green), opsonized with Alexa 488-labeled trastuzumab (pseudocolored red) and co-incubated with J774A.1 macrophages. Co-cultures were then incubated for 6 hours and imaged (fluorescence). E, MDA-MB-453 cancer cells opsonized with trastuzumab were co-incubated with J774A.1 macrophages that were preloaded with an equimolar mixture of pH-insensitive Alexa 488- and pH-sensitive pHrodo Red-labeled 10 kDa dextran (50 μg/mL each) for 1 hour followed by addition of 10 mg/mL IVIG and incubation for a further 6 hours. Fluorescent and DIC images are shown, with a line drawn across the phagosome/vacuole. Line intensity plot represents the normalized intensity between the 2 fluorescent signals (Alexa 488 and pHrodo Red, shown in blue and red, respectively) detected along the yellow line. Data for each fluorophore are normalized against the maximum signal level. The ratio of fluorescent intensities in the phagosomes and vacuoles were quantitated and 60% (n = 110) of vacuoles were found to have lower pHrodo Red:Alexa 488 intensity ratios compared with adjacent phagosomes. Yellow arrows in A, B, D and E indicate the location of the vacuole, and images of representative cells from at least 39 cells and 2 independent experiments are shown. Scale bars = 5 μm (A, B, D and E) or 1 μm (C)

was greater in torin 1-treated cells relative to control cells (Figure 5B). Fluorescence microscopy analyses also demonstrated that mTOR was present on the limiting LAMP-1+ membranes of the phagosome and associated vacuole for phagocytosed cancer cells (Figure 5C), consistent with mTOR activation.[37] By contrast, the levels of mTOR surrounding phagocytosed beads were substantially lower (Figure 5C). In addition, the intracellular levels of phosphorylated S6 (pS6) ribosomal protein, an indicator of mTOR activation, were analyzed in macrophages using an antibody specific for mouse/human pS6. Co-incubation of macrophages with antibody-opsonized tumor cells for 7 hours resulted in increased pS6 levels in macrophages compared with those in control samples or samples treated with torin 1 (Figure 5D). Taken together, these data suggest that although mTOR signaling occurs during phagosome/vacuole maturation following phagocytosis of cancer cells, inhibition of this pathway with torin 1 appears to affect phagosome/vacuole fission but does not prevent vacuole generation.

3 | DISCUSSION

In the current study, we describe a vacuolar structure that is formed during phagosomal maturation following macrophage-mediated phagocytosis of antibody-opsonized cancer cells. This vacuole is observed for 3 different macrophage:cancer cell combinations, suggesting that it is a universal structure associated with the phagocytic degradation of cellular targets. Although luminal space can be seen between the phagosomal "body" and the limiting membrane of the phagosome in earlier electron micrographs, the space appears to be contiguous with the phagosome.[3,30,38] By contrast, using EM and analyses of the differential accumulation of lysosomal tracers we demonstrate that the phagosome-associated vacuole described here is a discrete membrane-limited compartment (Figure 6).

Interestingly, LysoSensor Blue (DND-192) but not LysoTracker Red can be detected in the vacuole when these dyes are added shortly before microscopy analyses. However, fluorescence from both of these dyes, which are membrane permeant and localize to acidic compartments, is lower in the vacuole compared with the adjacent phagosome.[39] Two possibilities could explain this observation: First, the pH in the phagosome-associated vacuole may be higher than the pH in the phagosomal lumen. Our ratiometric analyses of the intensities of dextrans labeled with pH-sensitive and pH-insensitive fluors provide support for pH differences between the 2 compartments. Second, the entry of LysoTracker and LysoSensor into the vacuolar and phagosomal compartments may differ. For example, if the phagosome-associated vacuole is encapsulated by multiple membrane layers, acidic pH in the lumen between these membrane layers could result in accumulation of the acidotropic probes in this space and limit their diffusion into the vacuole. This possibility is supported by the detection of LysoTracker fluorescence surrounding the vacuole. Nevertheless, the higher fluorescent signal for LysoSensor relative to LysoTracker is likely to be due to the pH sensitivity of fluorescence of this dye.

We show that dextrans of distinct sizes are selectively excluded from the phagosome-associated vacuole. Differential sorting of molecules in macrophages has been previously observed to occur between lysosomes[32] and between lysosomes and phagosomes.[33,40] These studies led to the suggestion that such sorting might be caused by the diameter of the pores/tubules formed during potential kiss-and-run events that transfer solutes from one compartment to another.[41] Our data indicates that similar interconnections may exist between the phagosome and the associated vacuole. This is further supported by the exclusion of quantum dot nanoparticles from the vacuole.

While the function of the phagosome-associated vacuole appears to be primarily related to the controlled release of metabolites, additional functions may exist for this compartment. Early studies have suggested that the size of the phagosome may correlate with the quantity of metabolites it releases, due to excess osmotic pressure.[3] Similarly, the phagosome-associated vacuole could relieve such a buildup of osmotic pressure in a controlled manner. The differential accumulation of various solutes between the phagosome and the vacuole suggest that the vacuole may also act as a filter for the non-degradable or slowly degrading components of a large phagosome, separating and sequestering them from the degradable components. This possibility is supported by earlier reports suggesting that specialized lysosomal populations sequester such components.[42,43]

Antigen presenting cells that are active in cross-presentation have been shown to maintain a higher pH in the antigen-loading compartments than cells that do not cross-present their antigen, indicating that lower degradative rates are important for this process.[44–46] Interestingly, our data are consistent with a higher pH in the vacuole compared with the phagosome, suggesting that this compartment could play a role in cross-presentation. Although macrophages are typically regarded to be inefficient in this process, cross-presentation of antigen from target cells following ADCP has been reported.[24] Collectively, these observations suggest that the phagosome-associated vacuole may, therefore, be important for this pathway.

Analyses of mTOR and its downstream effector, pS6, demonstrate both mTOR association with the vacuole and increased pS6 levels in macrophages that contain antibody-opsonized tumor cells. This raises the question as to how the transcription factor, TFEB, which regulates the expression of a network of proteins involved in lysosomal biogenesis and function,[35,36] retains sufficient activity to support lysosome:phagosome formation, given that mTOR inhibits TFEB activation.[47,48] Several recent studies demonstrate that mTOR-independent pathways such as those involving Ca^{2+}-mediated signaling and the Ca^{2+} channel, transient receptor potential mucolipin 1 -(TRPML1, also known as MCOLN1), can play important roles in TFEB activation and lysosome:phagosome fusion.[9–11] Thus, the observation that phagosome/vacuole formation occurs despite mTOR activation suggests that alternative pathways leading to the enhancement of TFEB and lysosomal activity can override the counteracting effects of mTOR activation.[10,11,49]

In the current study, treatment of macrophage:cancer cell cultures with the mTOR inhibitor torin 1 does not inhibit vacuole formation, consistent with earlier studies demonstrating that torin 1 does not affect the formation of the entotic vacuole.[8] Instead, incubation

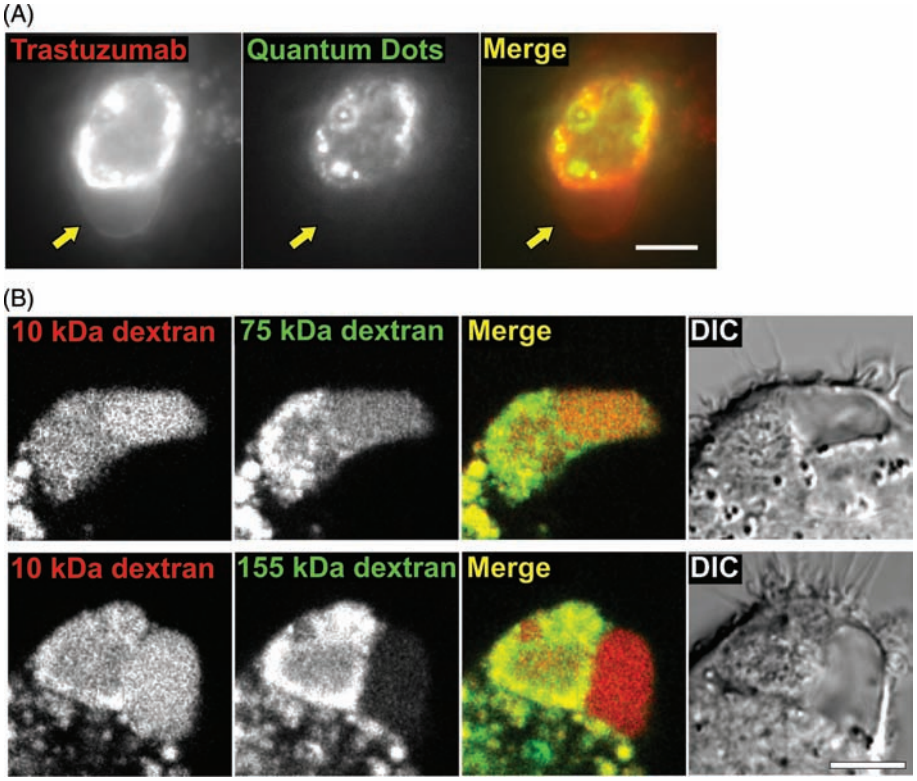

FIGURE 4 The vacuole is separated from the phagosome by a semi-permeable barrier. A, MDA-MB-453 cells were opsonized with Alexa 488-labeled trastuzumab (pseudocolored red) and counterstained with anti-human Fab-conjugated QDot 655 quantum dot nanoparticles (pseudocolored green). The cells were co-incubated with J774A.1 macrophages for 6 hours, followed by imaging (fluorescence). Yellow arrows indicate the location of the vacuole. B, MDA-MB-453 cells were opsonized with trastuzumab and co-incubated with J774A.1 macrophages for 6 hours followed by imaging (fluorescence and DIC). The macrophages were preloaded with Alexa 647-labeled 10 kDa dextran (pseudocolored red) and TRITC-labeled dextran of 75 or 155 kDa molecular weight (pseudocolored green) as indicated. Images of representative cells from at least 22 cells and 2 independent experiments are shown. Scale bars = 5 μm

of macrophages containing antibody-opsonized cancer cells with torin 1 results in the generation of larger vacuoles. By analogy with the behavior of entotic vacuoles,[8] this indicates that vacuole fission to reform lysosomes is inhibited by mTOR blockade. Based on our current analyses, however, we cannot exclude the possibility that mTOR inhibition also contributes to increased lysosome:phagosome fusion due to elevated TFEB activation. In this context, the identification of an mTOR-independent pathway for entotic vacuole fission involving PtdIns(3)P 5-kinase (PIK)fyve, a lipid kinase and its downstream effector, the Ca^{2+} channel TRPML1, indicate that this cation channel can play dual role in both the regulation of lysosomal activity and vacuole resolution.[9,10,12] Nevertheless, the increase in vacuole size that we observe in the presence of torin 1 suggests that the PIKfyve pathway cannot fully compensate for the negative effect of mTOR inhibition on vacuole fission.

The phagosome-associated vacuole appears to be specific for cellular targets since it was not observed for antibody-opsonized beads. A primary factor that differentiates cancer cells from other phagocytic targets such as beads is their composition, including the presence of phospholipids and high concentrations (200 g/L[50]) of proteins. The role of phospholipid intermediates in endosomal/lysosomal trafficking pathways,[51,52] combined with our data demonstrating that mTOR activation in response to released amino acids is not a prerequisite for vacuole generation, suggest that the presence of (phospho)lipids on the phagocytosed entity may be necessary for vacuole formation. It is also possible that the rigidity of the phagocytosed particle or cell affects vacuole development.

In summary, our study has identified a vacuole-like compartment that is associated with maturing phagosomes containing antibody-opsonized cells. Importantly, we demonstrate that this vacuole is separated by a semi-permeable membrane from the phagosome. Future studies will be directed towards defining the role of this vacuole in antigen presentation and other cellular processes related to phagocytosis.

4 | MATERIALS AND METHODS

4.1 | Cell lines and primary cells

The cell lines J774A.1 (Catalog no. TIB-67, RRID: CVCL_0358), SK-BR-3 (Catalog no. HTB-30, RRID: CVCL_0033), Raji (Catalog no. -CCL-86, RRID: CVCL_0511) and MDA-MB-453 (Catalog no. HTB-131, RRID: CVCL_0418) were purchased from the American Type Culture Collection. The cell lines were maintained in the following media supplemented with 10% fetal calf serum (FCS; Catalog no. 100-106, Gemini Bioproducts): macrophages and Raji cells, phenol red-free Dulbecco's Modified Eagle Medium (11965-092); MDA-MB-453, RPMI-1640 (11875-093); SK-BR-3, McCoy's (16600082). All experiments were conducted in medium containing FCS depleted of immunoglobulin G.[53] Long-term live imaging of macrophages was performed in Leibovitz's L-15 medium (11415-064) containing 10% FCS. Media were purchased from Thermo Fisher Scientific. Identities of the cancer cell lines were authenticated by short tandem repeat analysis (University of Arizona Genetics Core). Human monocytes were purchased frozen (Catalog no. 1008, Astarte Biologics) or were purified from peripheral blood mononuclear cells (kindly provided by Darrell Pilling, Texas A&M University) using the EasySep Human Monocyte Enrichment Kit (Catalog no. 19059, Stemcell Technologies). The monocytes were

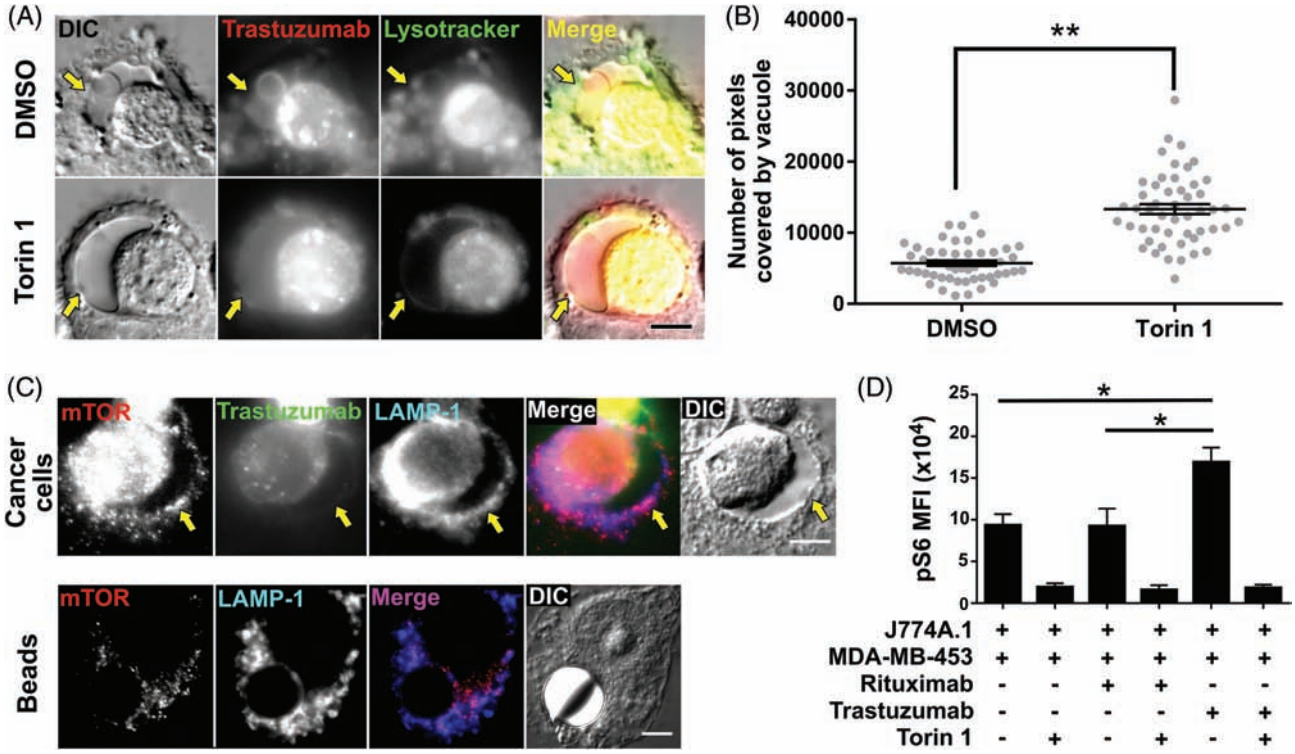

FIGURE 5 Inhibition of the mTOR pathway results in increased vacuole size. A, MDA-MB-453 cells opsonized with Alexa 488-labeled trastuzumab (pseudocolored red) were co-incubated with J774A.1 macrophages for 1 hour. The cells were then treated with 100 nM torin 1 or vehicle (DMSO) in the presence of 10 mg/mL IVIG and incubated for 6 hours. LysoTracker Red (pseudocolored green) was then added to the medium and cells were imaged. Fluorescent and DIC images show representative vacuoles observed for each treatment condition. B, the size of the vacuoles was quantitated by manually segmenting the areas positive for trastuzumab and negative for LysoTracker Red surrounding each phagosome (n = 50 vacuoles) and counting the number of pixels covered by these segmentations. Error bars represent SEs. The groups were compared using Student's t test, and ** indicates a statistically significant difference (P < .01). C, MDA-MB-453 cancer cells opsonized with Alexa 488-labeled trastuzumab (pseudocolored green) or streptavidin-coated beads (10 μm diameter) opsonized with biotinylated trastuzumab were co-incubated with J774A.1 macrophages for 1 hour followed by addition of 10 mg/mL IVIG and incubation for a further 6 hours. Cells were fixed, permeabilized and incubated with LAMP-1- and mTOR-specific antibodies followed by Alexa 647- and Alexa 555-labeled secondary antibodies, respectively. Fluorescent and DIC images are shown. D, MDA-MB-453 cells treated with trastuzumab, rituximab (anti-CD20) or no antibody (as indicated) were co-incubated with J774A.1 macrophages for 1 hour. The cells were then treated with 100 nM torin 1 or vehicle (DMSO) in the presence of 10 mg/mL IVIG and incubated for 6 hours, fixed, permeabilized, and incubated with FITC-labeled mouse CD45-specific antibody and rabbit antibody specific for pS6 followed by Alexa 647-labeled anti-rabbit (H+L) antibody. Averages of mean fluorescence intensities (MFIs) are shown for triplicate or quadruplicate samples with error bars indicating SD. One-way ANOVA analyses was carried out followed by a Tukey's multiple comparisons test between all sample pairs with a confidence interval of 95%. Horizontal lines indicate the groups compared and * indicates statistically significant differences (P < .05). Data shown are representative of 2 independent experiments. Yellow arrows in A and C indicate the location of the vacuole, and images of representative cells from at least 35 cells and 2 independent experiments are shown. Scale bars = 5 μm

cultured in DMEM containing 10% FCS supplemented with 50 ng/mL macrophage-colony stimulating factor (Catalog no. 300-25, Peprotech) in glass bottom dishes (MatTek corporation, Catalog no. P35G-1.5-10-C). Bone marrow-derived macrophages were isolated from C57BL/6J mice (purchased from The Jackson Laboratory) as described previously.[54]

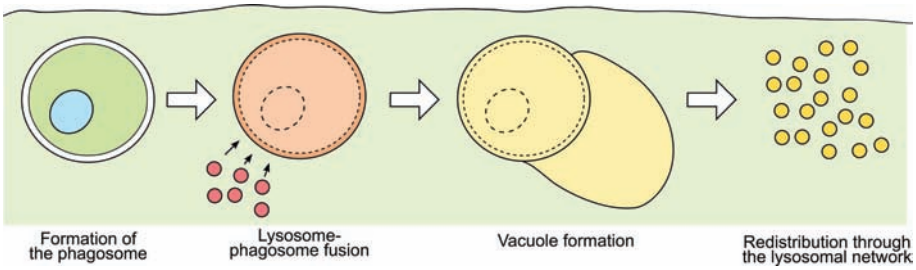

FIGURE 6 Schematic representation of the formation of the phagosome-associated vacuole. Following internalization of an antibody-opsonized cell, the lysosomes of the macrophage fuse with the phagosome. A distinct vacuole begins to form adjacent to the phagosome. Subsequently, the phagosome and the vacuole shrink and their constituents are redistributed throughout the lysosomal network of the macrophage

4.2 | Antibodies and other reagents

Clinical-grade trastuzumab, rituximab and IVIG (Gammunex) were obtained from the UT Southwestern Pharmacy. Trastuzumab and rituximab were labeled using Alexa 488 or 555 labeling kits (Thermo Fisher Scientific). The antibodies were labeled with 3-5 fluorophores per protein molecule. Trastuzumab was biotinylated as described previously.[55] LysoTracker Red (L7528), LysoSensor Blue DND-192, Alexa 488, 555, 647 and pHrodo Red-labeled dextran (10 kDa molecular weight; D-22910, D34679, D-22914 and P10361, respectively), FM 4-64FX (F34653), Alexa 555-labeled human transferrin (T35352), Alexa 647-labeled Annexin V (A23204), Alexa 488, 555 and 647-labeled goat anti-rabbit IgG (H+L) secondary antibody (A-11034; RRID: AB_2576217, A-21429; RRID: AB_141761 and A-21245; RRID: AB_2535813, respectively), Alexa 647-labeled goat anti-mouse IgG (H+L) secondary antibody (A-21236; RRID: AB_141725) and $F(ab')_2$-goat anti-human IgG (H+L) secondary antibody conjugated Qdot 655 nanoparticles (Q-11221MP; RRID: AB_2556468) were purchased from Thermo Fisher Scientific. Rabbit monoclonal antibodies specific for pS6 ribosomal protein (D68F8; Catalog no. 5364, RRID: AB_10694233), specific for phosphorylation at Ser240 and Ser244 residues and mTOR (Clone 7C10; Catalog no. 2983, RRID:AB_2105622) were purchased from Cell Signaling Technology. Rat anti-mouse LAMP-1 (Catalog no. 1D4B; RRID: AB_2134500) was purchased from the Developmental Studies Hybridoma Bank. Fluorescein isothiocyanate (FITC)-labeled rat anti-mouse CD45 (Clone 30-F11, Catalog no. 553079; RRID: AB_394609) was purchased from BD Biosciences. Tetramethylrhodamine isothiocyanate (TRITC)-labeled dextran with average molecular weights of 155 kDa (T1287) or 65 to 85 kDa (represented as 75 kDa; T1162) were purchased from Sigma-Aldrich. Torin 1 (235-t-7887) was purchased from LC Labs. Streptavidin-coated beads of 10 μm diameter (CP01N) were purchased from Bangs Laboratories. All experiments were performed in cells plated in MatTek glass bottom dishes.

4.3 | Sample pretreatment

For imaging phagosomes containing engulfed cancer cells, macrophages were first plated in MatTek glass bottom dishes. J774A.1 macrophages were plated overnight in the presence of 25 ng/mL murine interferon-γ (IFN-γ, Catalog no. 315-05, Peprotech). Mouse bone marrow-derived macrophages were similarly activated overnight with IFN-γ. Purified human monocytes were directly plated in MatTek glass bottom dishes 6 days prior to the experiment. Human macrophages were activated with human IFN-γ overnight. To label the lysosomes of macrophages with dextran, the macrophages were incubated with medium containing 100 μg/mL labeled dextran for 1 hour, washed and incubated with medium for 2 to 4 hours prior to the addition of target cells. To label cancer cell lysosomes with dextran, cells were either pulse-chased (2 hours pulse, 4 hours chase) or incubated for 12 hours with 100 μg/mL dextran, followed by incubation with medium for 4 hours prior to addition to the macrophages.

4.4 | Phagocytosis of cancer cells by macrophages

The cancer cells were harvested from flasks by mild trypsinization, washed and incubated with 10 μg/mL labeled opsonizing antibody for 10 minutes at room temperature. The cells were then washed twice with PBS followed by re-suspension in medium. Cancer cells were added to macrophages at 1:0.875 effector:target ratios (35000 target cells were added to 40000 plated macrophages in 10 mm MatTek glass bottom dishes) and incubated for various time points before imaging. When indicated in the figure legends, the medium in the dishes was replaced with medium containing 10 mg/mL IVIG to block further phagocytosis following 1 hour of co-culture. In a subset of experiments, LysoTracker Red (2 nM) and LysoSensor Blue (50 nM) were added to the medium and incubated at room temperature for 5 minutes to label the acidic compartments. For immunofluorescence using J774A.1 macrophages, cells were fixed in 1:1 methanol:acetone at −20°C for 5 minutes.

4.5 | Flow cytometry analyses

For flow cytometry analyses, co-cultures of macrophages and cancer cells were prepared as described above. One hour later, 10 mg/mL IVIG was added to block further phagocytosis and cells were treated with 100 nM torin 1 or vehicle (DMSO) for an additional 6 hours. As controls, MDA-MB-453 cells treated with rituximab (anti-CD20) and MDA-MB-453 cells without antibody were used. Following the incubation, cells were harvested, fixed with 2% paraformaldehyde for 10 minutes at 37°C, permeabilized with methanol for 30 minutes at −20°C, and stained with FITC-labeled mouse CD45-specific antibody and rabbit monoclonal antibody specific for pS6. Alexa 647-labeled anti-rabbit antibody was used to detect the pS6-specific antibody. Following staining and washing, stained cells were analyzed using flow cytometry (Accuri). Flow cytometry data were processed using FlowJo software (FlowJo, RRID: SCR_008520).

4.6 | EM sample preparation

Cells were fixed on gridded MatTek dishes (Catalog no. P35G-1.5-14-CGRD-D) with 2.5% (v/v) glutaraldehyde in 0.1 M sodium cacodylate buffer. After 3 rinses in 0.1 M sodium cacodylate buffer, they were post-fixed in 1% osmium tetroxide and 0.8% $K_3[Fe(CN_6)]$ in 0.1 M sodium cacodylate buffer for 1 hour at room temperature. Cells were rinsed with water and en bloc stained with 2% aqueous uranyl acetate overnight. After 3 rinses with water, specimens were dehydrated with increasing concentrations of ethanol, infiltrated with Embed-812 resin and polymerized in a 60°C oven overnight. Blocks were sectioned with a diamond knife (Diatome) on a Leica Ultracut UC7 ultramicrotome (Leica Microsystems) and collected on copper grids, followed by post-staining with 2% uranyl acetate in water and lead citrate. Images were acquired using a Tecnai G2 Spirit transmission electron microscope (FEI) equipped with a LaB6 source using a voltage of 120 kV.

4.7 | Microscope configurations

For single time-point imaging, images were acquired using a Zeiss Axiovert 200M inverted fluorescence microscope with a Zeiss 63x/1.4NA Plan Apochromat objective as described previously.[56] Long-term live imaging of the formation of the vacuole was imaged

using a Zeiss Axio Observer.A1 body and a Zeiss 63x/1.4NA Plan Apochromat objective. The sample was illuminated with a 488-nm solid-state laser (Coherent) for Alexa 488 excitation and a 543-nm diode laser (Opto Engine LLC) for Alexa 555 excitation. The illumination was directed to the sample and fluorescence filtered back using a polychroic beam splitter/emission filter combination (488/543/633 RPC and 488/543M; Chroma Technology Corporation). The fluorescence emission was detected using an Andor iXon EMCCD camera (Andor Technologies). The cameras were run on conventional gain mode and images were acquired in 2 colors along with a transmitted light image at an acquisition rate of 1 block per minute. Camera acquisition and shuttering of excitation lasers were controlled using custom acquisition software written in LabWindows/CVI (National Instruments Corporation). The acquired images were registered and processed using the microscopy image analysis tool (http://wardoberlab.com/software/miatool)[57] implemented in MATLAB (MathWorks, Inc; RRID: SCR_001622). The temperature and humidity in the microscope system were maintained by a caged temperature-control system (OKOlabs). Long-term imaging of the degradation of the vacuoles, the imaging of LysoSensor and of the different molecular weight dextrans were performed using a Nikon A1R confocal microscope equipped with a 60X 1.4 NA Plan Apo objective and a temperature-control system. The acquired images were exported to TIFF format and processed with microscopy image analysis tool as described above.

4.8 | Statistical analyses

Tests for statistical significance between groups were carried out using Student's *t* test or one-way analysis of variance (ANOVA) with Tukey's multiple comparison test in GraphPad Prism, V6.0 (GraphPad Software. Inc http://www.graphpad.com, RRID: SCR_002798). *P*-values of less than .05 were considered to be significant.

ACKNOWLEDGEMENTS

We thank Dr Darrell Pilling (Texas A&M University) for providing peripheral blood mononuclear cell samples and Dr Chandrashekhar Pasare (University of Texas Southwestern Medical Center, Dallas) for assistance with the isolation of mouse macrophages. We are grateful to Dr Dilip K. Challa for helpful suggestions and Dr Min Mo for assistance with flow cytometry analyses. We thank the Department of Molecular & Cellular Medicine (Texas A&M University Health Science Center) for providing access to the confocal microscope facility. We also thank the University of Texas Southwestern Medical Center EM core facility and Harold R. Payne from the Texas A&M College of Veterinary Medicine Image Analysis Laboratory for EM sample preparation and imaging services.

This research was supported in part by grants from the Cancer Prevention and Research Institute of Texas (RP140141 awarded to E.S.W., RP110441 awarded to E.S.W. and R.J.O.) and the National Institutes of Health (R01GM085575, awarded to R.J.O.).

Conflict of interest

The authors declare no conflict of interest.

Editorial Process File: The Editorial Process File is available in the online version of this article.

ORCID

E. Sally Ward http://orcid.org/0000-0002-9311-8571

REFERENCES

1. Freeman SA, Grinstein S. Phagocytosis: receptors, signal integration, and the cytoskeleton. *Immunol Rev*. 2014;262(1):193-215.
2. Flannagan RS, Jaumouillé V, Grinstein S. The cell biology of phagocytosis. *Annu Rev Pathol*. 2012;7(1):61-98.
3. Segal AW, Geisow M, Garcia R, Harper A, Miller R. The respiratory burst of phagocytic cells is associated with a rise in vacuolar pH. *Nature*. 1981;290(5805):406-409.
4. Saxton RA, Sabatini DM. mTOR signaling in growth, metabolism, and disease. *Cell*. 2017;168(6):960-976.
5. Puertollano R. mTOR and lysosome regulation. *F1000Prime Rep*. 2014;6(52):52.
6. Zoncu R, Bar-Peled L, Efeyan A, Wang S, Sancak Y, Sabatini DM. mTORC1 senses lysosomal amino acids through an inside-out mechanism that requires the vacuolar H(+)-ATPase. *Science*. 2011;334(6056):678-683.
7. Overholtzer M, Brugge JS. The cell biology of cell-in-cell structures. *Nat Rev Mol Cell Biol*. 2008;9(10):796-809.
8. Krajcovic M, Krishna S, Akkari L, Joyce JA, Overholtzer M. mTOR regulates phagosome and entotic vacuole fission. *Mol Biol Cell*. 2013;24(23):3736-3745.
9. Dayam RM, Saric A, Shilliday RE, Botelho RJ. The phosphoinositide-gated lysosomal Ca^{2+} channel, TRPML1, is required for phagosome maturation. *Traffic*. 2015;16(9):1010-1026.
10. Gray MA, Choy CH, Dayam RM, et al. Phagocytosis enhances lysosomal and bactericidal properties by activating the transcription factor TFEB. *Curr Biol*. 2016;26(15):1955-1964.
11. Martina JA, Diab HI, Brady OA, Puertollano R. TFEB and TFE3 are novel components of the integrated stress response. *EMBO J*. 2016;35(5):479-495.
12. Krishna S, Palm W, Lee Y, et al. PIKfyve regulates vacuole maturation and nutrient recovery following engulfment. *Dev Cell*. 2016;38(5):536-547.
13. Scott AM, Wolchok JD, Old LJ. Antibody therapy of cancer. *Nat Rev Cancer*. 2012;12(4):278-287.
14. Braster R, O'Toole T, van Egmond M. Myeloid cells as effector cells for monoclonal antibody therapy of cancer. *Methods*. 2014;65(1):28-37.
15. Weiskopf K, Weissman IL. Macrophages are critical effectors of antibody therapies for cancer. *MAbs*. 2015;7(2):303-310.
16. Noy R, Pollard JW. Tumor-associated macrophages: from mechanisms to therapy. *Immunity*. 2014;41(1):49-61.
17. Velmurugan R, Challa DK, Ram S, Ober RJ, Ward ES. Macrophage -mediated trogocytosis leads to death of antibody-opsonized tumor cells. *Mol Cancer Ther*. 2016;15(8):1879-1889.
18. Shi Y, Fan X, Deng H, et al. Trastuzumab triggers phagocytic killing of high HER2 cancer cells in vitro and in vivo by interaction with Fcγ receptors on macrophages. *J Immunol*. 2015;194(9):4379-4386.
19. Leidi M, Gotti E, Bologna L, et al. M2 macrophages phagocytose rituximab-opsonized leukemic targets more efficiently than M1 cells in vitro. *J Immunol*. 2009;182(7):4415-4422.
20. Chao MP, Alizadeh AA, Tang C, et al. Anti-CD47 antibody synergizes with rituximab to promote phagocytosis and eradicate non-Hodgkin lymphoma. *Cell*. 2010;142(5):699-713.
21. Grugan KD, McCabe FL, Kinder M, et al. Tumor-associated macrophages promote invasion while retaining Fc-dependent anti-tumor function. *J Immunol*. 2012;189(11):5457-5466.
22. Gul N, Babes L, Siegmund K, et al. Macrophages eliminate circulating tumor cells after monoclonal antibody therapy. *J Clin Invest*. 2014;124(2):812-823.

23. Overdijk MB, Verploegen S, Bogels M, et al. Antibody-mediated phagocytosis contributes to the anti-tumor activity of the therapeutic antibody daratumumab in lymphoma and multiple myeloma. *MAbs*. 2015;7(2):311-321.
24. Tseng D, Volkmer JP, Willingham SB, et al. Anti-CD47 antibody -mediated phagocytosis of cancer by macrophages primes an effective antitumor T-cell response. *Proc Natl Acad Sci U S A*. 2013; 110(27):11103-11108.
25. Mantegazza AR, Magalhaes JG, Amigorena S, Marks MS. Presentation of phagocytosed antigens by MHC class I and II. *Traffic*. 2013;14(2): 135-152.
26. Pham T, Mero P, Booth JW. Dynamics of macrophage trogocytosis of rituximab-coated B cells. *PLoS One*. 2011;6(1):e14498.
27. Beum PV, Mack DA, Pawluczkowycz AW, Lindorfer MA, Taylor RP. Binding of rituximab, trastuzumab, cetuximab, or mAb T101 to cancer cells promotes trogocytosis mediated by THP-1 cells and monocytes. *J Immunol*. 2008;181(11):8120-8132.
28. Chazotte B. Labeling lysosomes in live cells with LysoTracker. *Cold Spring Harb Protoc*. 2011;2011(2):pdb.prot5571.
29. Lin HJ, Herman P, Kang JS, Lakowicz JR. Fluorescence lifetime characterization of novel low-pH probes. *Anal Biochem*. 2001;294(2): 118-125.
30. Brooks CR, Yeung MY, Brooks YS, et al. KIM-1-/TIM-1-mediated phagocytosis links ATG5-/ULK1-dependent clearance of apoptotic cells to antigen presentation. *EMBO J*. 2015;34(19):2441-2464.
31. Panchuk-Voloshina N, Haugland RP, Bishop-Stewart J, et al. Alexa dyes, a series of new fluorescent dyes that yield exceptionally bright, photostable conjugates. *J Histochem Cytochem*. 1999;47(9):1179 -1188.
32. Spence MTZ, Johnson ID, eds. *The Molecular Probes Handbook: A Guide to Fluorescent Probes and Labeling Technologies*. 11th ed., Life Technologies, Carlsbad, CA, 2010.
33. Kasmapour B, Gronow A, Bleck CKE, Hong W, Gutierrez MG. Size-dependent mechanism of cargo sorting during lysosome -phagosome fusion is controlled by Rab34. *Proc Natl Acad Sci U S A*. 2012;109(50):20485-20490.
34. Berthiaume EP, Medina C, Swanson JA. Molecular size-fractionation during endocytosis in macrophages. *J Cell Biol*. 1995;129(4):989-998.
35. Settembre C, Di Malta C, Polito VA, et al. TFEB links autophagy to lysosomal biogenesis. *Science*. 2011;332(6036):1429-1433.
36. Sardiello M, Palmieri M, di Ronza A, et al. A gene network regulating lysosomal biogenesis and function. *Science*. 2009;325(5939):473-477.
37. Sancak Y, Bar-Peled L, Zoncu R, Markhard AL, Nada S, Sabatini DM. Ragulator-Rag complex targets mTORC1 to the lysosomal surface and is necessary for its activation by amino acids. *Cell*. 2010;141(2): 290-303.
38. Muraille E, Gounon P, Cazareth J, et al. Direct visualization of peptide/MHC complexes at the surface and in the intracellular compartments of cells infected in vivo by Leishmania major. *PLoS Pathog*. 2010;6(10):e1001154.
39. Han J, Burgess K. Fluorescent indicators for Intracellular pH. *Chem Rev*. 2010;110(5):2709-2728.
40. Desjardins M, Nzala NN, Corsini R, Rondeau C. Maturation of phagosomes is accompanied by changes in their fusion properties and size-selective acquisition of solute materials from endosomes. *J Cell Sci*. 1997;110(pt 18):2303-2314.
41. Bright NA, Davis LJ, Luzio JP. Endolysosomes are the principal intracellular sites of acid hydrolase activity. *Curr Biol*. 2016;26(17): 2233-2245.
42. Tassin MT, Lang T, Antoine JC, Hellio R, Ryter A. Modified lysosomal compartment as carrier of slowly and non-degradable tracers in macrophages. *Eur J Cell Biol*. 1990;52(2):219-228.
43. Astarie-Dequeker C, Carreno S, Cougoule C, Maridonneau-Parini I. The protein tyrosine kinase Hck is located on lysosomal vesicles that are physically and functionally distinct from CD63-positive lysosomes in human macrophages. *J Cell Sci*. 2002;115(pt 1):81-89.
44. Alloatti A, Kotsias F, Magalhaes JG, Amigorena S. Dendritic cell maturation and cross-presentation: timing matters! *Immunol Rev*. 2016; 272(1):97-108.
45. Yates RM, Hermetter A, Taylor GA, Russell DG. Macrophage activation downregulates the degradative capacity of the phagosome. *Traffic*. 2007;8(3):241-250.
46. Cohn L, Chatterjee B, Esselborn F, et al. Antigen delivery to early endosomes eliminates the superiority of human blood BDCA3+ dendritic cells at cross presentation. *J Exp Med*. 2013;210(5):1049-1063.
47. Martina JA, Chen Y, Gucek M, Puertollano R. mTORC1 functions as a transcriptional regulator of autophagy by preventing nuclear transport of TFEB. *Autophagy*. 2012;8(6):903-914.
48. Roczniak-Ferguson A, Petit CS, Froehlich F, et al. The transcription factor TFEB links mTORC1 signaling to transcriptional control of lysosome homeostasis. *Sci Signal*. 2012;5(228):ra42.
49. Palmieri M, Pal R, Nelvagal HR, et al. mTORC1-independent TFEB activation via Akt inhibition promotes cellular clearance in neurodegenerative storage diseases. *Nat Commun*. 2017;8:14338.
50. Milo R. What is the total number of protein molecules per cell volume? A call to rethink some published values. *Bioessays*. 2013;35(12): 1050-1055.
51. Bohdanowicz M, Grinstein S. Role of phospholipids in endocytosis, phagocytosis, and macropinocytosis. *Physiol Rev*. 2013;93(1):69-106.
52. Dove SK, Dong K, Kobayashi T, Williams FK, Michell RH. Phosphatidylinositol 3,5-bisphosphate and Fab1p/PIKfyve underPPIn endolysosome function. *Biochem J*. 2009;419(1):1-13.
53. Ober RJ, Martinez C, Vaccaro C, Zhou J, Ward ES. Visualizing the site and dynamics of IgG salvage by the MHC class I-related receptor, FcRn. *J Immunol*. 2004;172(4):2021-2029.
54. Lin K-M, Hu W, Troutman TD, et al. IRAK-1 bypasses priming and directly links TLRs to rapid NLRP3 inflammasome activation. *Proc Natl Acad Sci U S A*. 2014;111(2):775-780.
55. Vaccaro C, Bawdon R, Wanjie S, Ober RJ, Ward ES. Divergent activities of an engineered antibody in murine and human systems have implications for therapeutic antibodies. *Proc Natl Acad Sci U S A*. 2006;103(49):18709-18714.
56. Gan Z, Ram S, Vaccaro C, Ober RJ, Ward ES. Analyses of the recycling receptor, FcRn, in live cells reveal novel pathways for lysosomal delivery. *Traffic*. 2009;10(5):600-614.
57. Chao J, Ward ES, Ober RJ. A software framework for the analysis of complex microscopy image data. *IEEE Trans Inf Technol Biomed*. 2010; 14(4):1075-1087.

SUPPORTING INFORMATION

Additional Supporting Information may be found online in the supporting information tab for this article.

How to cite this article: Velmurugan R, Ramakrishnan S, Kim M, Ober RJ, Ward ES. Phagocytosis of antibody-opsonized tumor cells leads to the formation of a discrete vacuolar compartment in macrophages. *Traffic*. 2018;19: 273–284. https://doi.org/10.1111/tra.12552